Chinese Chemical Letters 35 (2024) 109233

Contents lists available at ScienceDirect

Chinese Chemical Letters

journal homepage: www.elsevier.com/locate/cclet

A stable radiochromic semiconductive viologen-based metal–organic framework for dual-mode direct X-ray detection

Xuying Yu[a,c], Jiarong Mi[a,b], Yulan Han[d], Cai Sun[b], Mingsheng Wang[a,*], Guocong Guo[a,*]

[a] State Key Laboratory of Structural Chemistry, Fujian Institute of Research on the Structure of Matter, Chinese Academy of Sciences, Fuzhou 350608, China
[b] College of Chemistry, Fuzhou University, Fuzhou 350108, China
[c] University of Chinese Academy of Sciences, Beijing 100049, China
[d] School of Chemistry and Chemical Engineering, Queen's University Belfast, Belfast BT9 5AG, United Kingdom

ARTICLE INFO

Article history:
Received 18 September 2023
Revised 16 October 2023
Accepted 23 October 2023
Available online 24 October 2023

Keywords:
Metal-organic framework
Viologen
Photochromism
Conductance
X-ray detection

ABSTRACT

Direct X-ray detectors, which directly convert X-rays into electrical signals through semiconductors, have higher space solution than scintillator-mediated indirect X-ray ones and are high desirable for early cancer detection and other applications, but the mainstream commercial α-Se detector is still largely limited by high production costs, large leakage current and low stability. This article reports an easily prepared, stable radiochromic semiconductive metal–organic framework (MOF), $(MV)[Cd_3(tdc)_4]\cdot 2H_2O$ (RCS-1, H_2tdc = 2,5-thiophenedicarboxylic acid; MV^{2+} = methyl viologen cation) with direct X-ray detecting ability. With a large bulk resistivity of 8.40×10^9 Ω cm, this material ensures minimal dark current and low noise for X-ray detection. Additionally, it exhibits higher sensitivity to W Kα X-rays (98.58 μC Gy^{-1} cm^{-2}) than α-Se (~20 μC Gy^{-1} cm^{-2}). Meanwhile, unlike most reported direct X-ray detecting semiconductors, compound RCS-1 shows remarkable color change upon X-ray irradiation owing to the presence of photochromism-active viologen cations. This feature offers an appealing visual detecting ability to direct X-ray detectors that provide only the electrical signals.

X-ray detection plays a crucial role in various fields, including scientific research, medical diagnosis, safety inspection and astrophysics [1–3]. The main detection methods include indirect and direct types [4]. Scintillator detectors can transform X-rays into a burst of visible light, which is then converted into the electrical signals [5]. They have widespread applications because of good stability, high conversion rate, and low cost, but insufficient spatial resolution makes them ineffective for early screening of cancers such as breast cancer [6,7]. Compared with scintillator detectors, semiconductor detectors offer better spatial resolution and a simpler route [8,9]. They have been successfully used for early screening of cancers [10]. However, current commercial products are largely limited by high production costs and low stability. Additionally, semiconductor detectors lack the ability to directly visualize detection and imaging results through color changes, unlike silver-based photosensitive films that can [11]. Radiochromic semiconductors possess the dual capability of displaying electrical signals and color changes, meeting the requirements for dual X-ray detection [12]. However, to date, only one case has been reported, and it is still subject to low X-ray absorption efficiency [13].

Metal−organic frameworks (MOFs) provide a good platform for designing radiochromic semiconductors [14–19]. One way to design radiochromic semiconductive MOFs is by constructing a carrier transport path through the introduction of an optically active organic guest molecule [20,21]. Viologens and their analogues are known for their good properties, including photochromism and reversible radiochromism [22,23]. The viologens unit, as a guest in the framework, forms channels for transporting electrons with conjugation and enhances the capacity for carrying transport [24,25]. This molecule may exhibit color change after radiation and simultaneously modulate the charge carrier density of the semiconducting MOF skeleton [26,27]. On the contrary, the porous structure of MOF also serves to minimize direct contact between viologen radicals and air, thereby ensuring the stability of discoloration products. This is a promising strategy for building radiochromic semiconductive materials. Based on the aforementioned strategy, we synthetized a radiochromic semiconductive MOF through a one−pot method, namely $(MV)[Cd_3(tdc)_4]\cdot 2H_2O$ (RCS-1; H_2tdc = 2,5-thiophenedicarboxylic acid, MV^{2+} = methyl viologen cation). RCS-1 exhibits both a photocurrent signal and clear color change upon exposure to X-rays. Its detection sensitivity is

* Corresponding authors.
E-mail addresses: mswang@fjirsm.ac.cn (M. Wang), gcguo@fjirsm.ac.cn (G. Guo).

https://doi.org/10.1016/j.cclet.2023.109233
1001-8417/

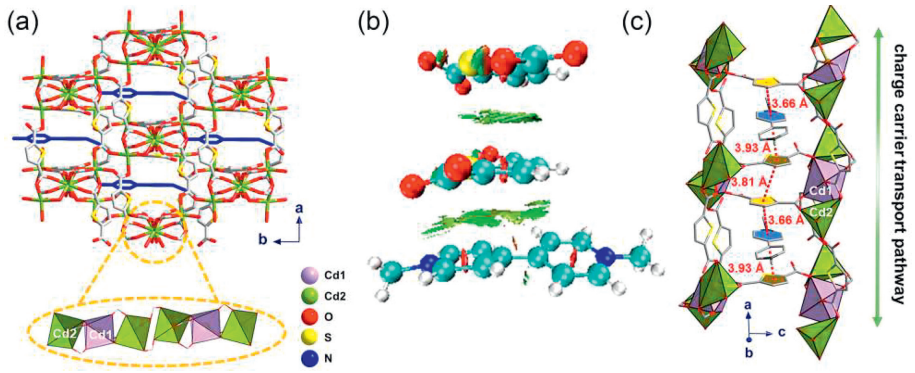

Fig. 1. Crystal structure of RCS-1: (a) 3D open framework viewed along the *c* direction. (b) Color-filled RDG map for the π-aggregated motifs. (c) π-stacking interactions (dash lines) along the *a* direction. Hydrogen atoms are omitted for clarity in (a) and (c).

98.85 μC Gy^{-1} cm^{-2} under the bias voltage of 30 V, which surpasses those of commercial α-Se detectors (~20 μC Gy^{-1} cm^{-2}). Moreover, RCS-1 possesses large bulk resistivity of 8.40×10^9 Ω cm comparable to that of commercial CZT detector (10^9–10^{11} Ω cm), ensuring low dark current and noise for X-ray detection. Additionally, this material demonstrates good thermal stable and X-ray irradiation stability as its detection performance does not attenuate after prolonged exposure to X-rays.

A single crystal X-ray diffraction study revealed that RCS-1 crystallizes in the *C*2/c space group [28]. Its asymmetric unit consists of two fully deprotonated tdc^{2-} ligands, one free H_2O molecules, one and a half Cd(II) ions and half of a MV^{2+} ion as guest molecule in the channel (Fig. S1a in Supporting information). Cd(II) ions has two coordination modes, with Cd1 being six-coordinated and Cd2 being five-coordinated. The carboxylate groups of tdc^{2-} ligands connect Cd(II) ions to generate an infinite rod-shaped building block [29]. These blocks are further connected by the thiophene groups of the tdc^{2-} ligands to yield an anionic open framework with channels extending to the *c* direction (Fig. 1a). The channels are filled with the MV^{2+} ions for valence balance. And in this structure, the methyl groups of MV^{2+} were disordered, and the attempts to locate and refine it were successful (Fig. S1b in Supporting information).

A reduced density gradient (RDG) analysis (Fig. 1b) illustrates the presence of π-π interactions (represented by the green region) between two adjacent thiophene rings or between MV^{2+} and its adjacent two thiophene rings [30]. Each MV^{2+} cation interacts two adjacent thiophene rings through π-π interactions (mean centroid-to-centroid separation: 3.80 Å) to form a π aggregate. Such π aggregates are further linked with the help of π-π interactions (centroid-to-centroid separation: 3.81 Å) between two terminal thiophene rings to yield an infinite π-stacking chain along the *a* direction (Fig. 1c). These π-stacking chains contribute to the carrier transmission, prompting us to further explore its electronic applications.

The dark current is primarily determined by the intrinsic carrier concentration, which in turn depends on the band gap of the material. A direct band gap was revealed through band structure calculations for RCS-1 (Fig. 2a). The optical band gap, calculated using the Tauc plot, $(\alpha h\nu)^2 = A(h\nu - E_g)$ [31], was found to be 2.68 eV (Fig. 2b), falling within the appropriate range (1.50–3.0 eV) for radiation detection application [32]. Density of states (DOS) analysis reveals the valence band maximum and the conduction band minimum of RCS-1 are contributed mainly by tdc^{2-} and MV^{2+} [33].

The X-ray detection performance of the RCS-1 was investigated by initially assessing its attenuation coefficients across the 1–100 keV range, utilizing the XCOM photon cross section database [34]. This energy range is typical for medical imaging purposes. For comparison, traditional direct X-ray materials α-Se, Cd(Zn)Te (CZT),

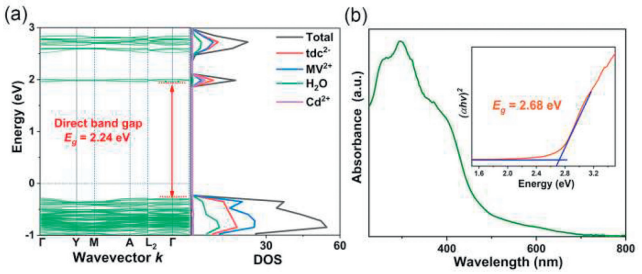

Fig. 2. Electron structure of RCS-1: (a) Band structure and DOS. (b) UV–vis absorption spectrum; inset: The Tauc plot.

and Si are included. As depicted in Fig. 3a, RCS-1 has an absorption coefficient similar to that of α-Se at the 59.3 keV photon energy for the W-$K_{\alpha 1}$ X ray, which can be attributed to its high atomic number and density (11.01 g/cm^3). The detector's test only requires a thickness of 0.24 mm, thanks to the high X-ray attenuation efficiency of 97% provided by commercial Si detector (Fig. 3b).

Considerring the good X-ray attenuation effciency, we studied the X-ray detection performance of RCS-1. The phase purity of the bulk sample was first evaluated by power X-ray diffraction (PXRD) before electrical tests. A pellet-based X-ray detector device with an Ag/sample/Ag structure was fabricated for RCS-1 to evaluate its behavior for the intrinsic carrier transport (Fig. 3c) [35]. The current–voltage (*I*–*V*) curve for RCS-1 showed a symmetrical linear relationship within the voltage range of −20 V to +20 V. An impressive bulk resistivity of 8.40×10^9 Ω cm was obtained. This value is comparable to that of commercial CZT detectors (10^9–10^{11} Ω cm) [36,37], ensuring low dark current and noise levels during X-ray detection (Fig. 3d). As can be also seen from Fig. 3d, the photocurrent raises quickly as the X-ray dose rate increases, which indicates efficient charge carrier generation in RCS-1.

RCS-1 detector exhibited a clear photocurrent response upon irradiation of the tungsten anode (W) X-ray at a bias voltage of 30 V, and the intensity of the photocurrent increased with an increase in the dose rate (Fig. S3 in Supporting information). This demonstrates that high dose rate X-rays significantly enhance the concentrations of charge carriers, leading to a higher photocurrent. The sensitivity of a direct-type X-ray detector is a crucial parameter that characterizes its ability to respond to a specific level of irradiation [38]. A high sensitivity indicates that the detector can generate a large photocurrent when exposed to a given dose rate of X-rays, and it plays an important role in determining the imaging quality. Generally, the detection sensitivity (*S*) is defined as the fitting data of ratio of the current density to dose rate [39]. The *S* value of the RCS-1 detector under a tube voltage of 50 KV_p and a bias voltage of 30 V is 98.85 μC Gy^{-1} cm^{-2} (Fig. 3f). This value is higher than that

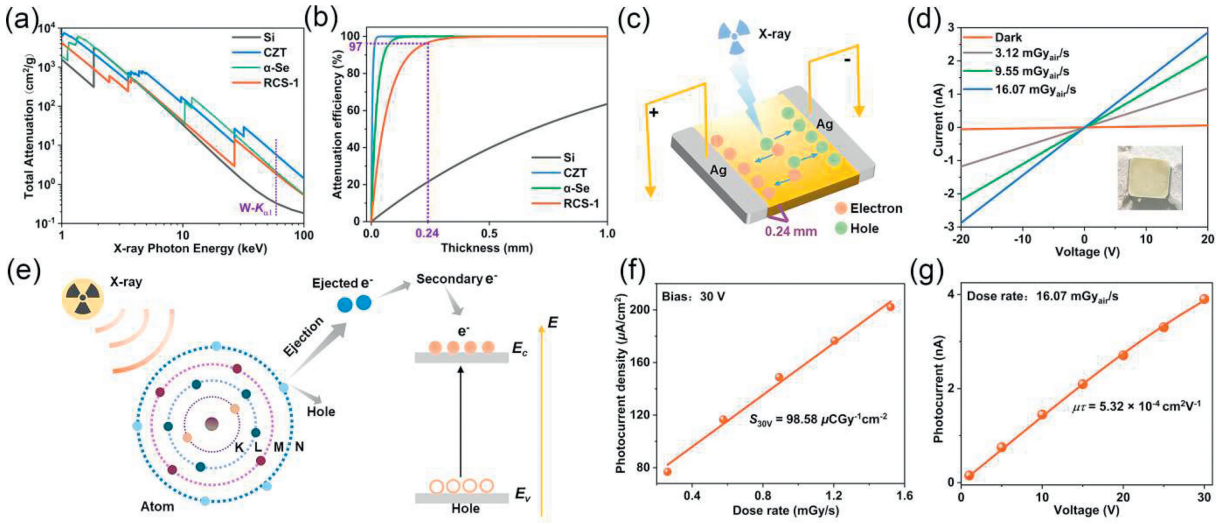

Fig. 3. X-ray detection performance of RCS-1: (a) Calculated mass attenuation coefficients and (b) thickness dependent attenuation efficiency. Commercial X-ray detection materials Cd(Zn)Te, *a*-Se and Si are included for comparison. (c) Schematic illustration of the pellet X-ray detector. (d) *I*–*V* curves under the X-ray off and on with different exposed dose rates and actual electrode diagram (inset). (e) Mechanism for X-ray photon to current conversion. (f) Photocurrent density *versus* dose rate measured at a bias voltage of 30 V. (g) Voltage-dependent photocurrent curves fitted by the Hecht equation.

of the commercial α-Se detectors (~20 μC Gy^{-1} cm^{-2}). Additionally, we evaluated the charge carrier mobility and lifetime product ($\mu\tau$). The large $\mu\tau$ product ensures a high transmission speed of X-ray generated carriers and reduces their recombination due to aggregation, thereby guaranteeing a high charge-collection efficiency under a low electric field [40]. This value was measured to be 5.32 × 10^{-4} cm^2/V, which is significantly higher than that of commercially availavble α-Se detectors (~10^{-7} cm^2/V) and comparable to uncommercial perovskite (~10^{-7} – 10^{-2} cm^2/V) and MOF (~10^{-4} cm^2/V) detectors (Fig. 3g) [41]. Furthermore, by alternately activating and deactivating the X-ray source, we demonstrated remarkable operational stability across various bias voltages using *I*–*t* curves (Fig. S4 in Supporting information). Under our instrument's lowest dose rate of 0.11 μGy$_{air}$/s, RCS-1 achieved a signal-to-noise ratio (SNR) of 40.18, indicating its ability to detect even smaller doses.

The performance of X-ray detectors is determined by not only their X-ray absorption efficiency but also their ability to separate and transport the generated charge [42,43]. Fig. 3e illustrates the potential mechanism for the detection process of RCS-1. When X-rays interact with RCS-1, the photoelectric effect is triggered and results in the generation of high-energy electron-hole pairs. Some electrons and holes undergo recombination or energy dissipation as a result of their mutual interactions. Subsequently, most of them migrate to the conduction band while leaving behind holes in the valence band. Finally, surviving electrons and holes move towards opposite electrodes under a certain electric field and generate a current signal. It is well known that multiple strong π-π intermolecular interactions in the material's structure favor carrier transport [44]. RCS-1 possesses an extended conjugated π-electron delocalization area which reduces energy loss during carrier transport and enables rapid carrier transfer within its structure.

Cu-K$_\alpha$ (λ = 1.54056 Å) and Al-K$_\alpha$ (λ = 8.357 Å) X-rays were utilized to investigate the radiochromic properties of RCS-1. Upon irradiation, the sample exhibited a noticeable color change (Fig. 4a and Fig. S5 in Supporting information), gradually shifting from yellow to blue over a period of 10 min and 30 s, respectively. As the irradiation time increased, the blue hue deepened. Following exposure to Cu-K$_\alpha$ X-ray radiation, the blue sample displayed characteristic absorption bands for viologen monoradicals at approximately 360 and 610 nm (Fig. 4b) [45]. A sharp single-line signal at 3518 Gauss (g = 2.003, linewidth = 19 Gauss) in the EPR spectrum con-

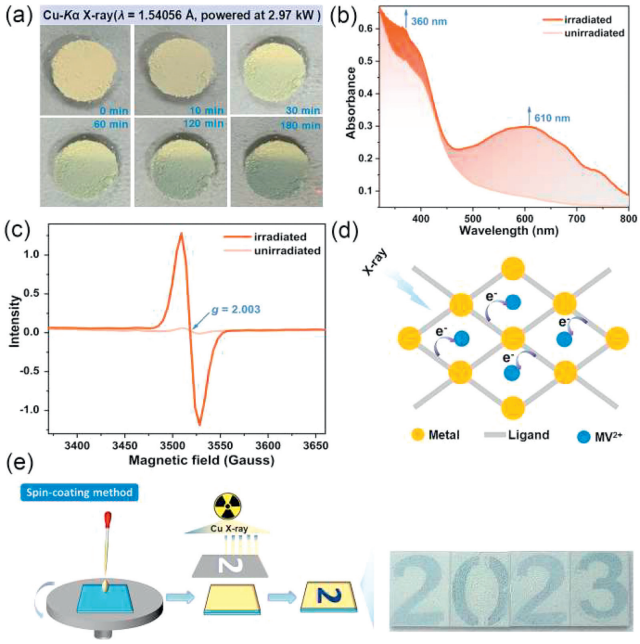

Fig. 4. Radiochromic behavior for RCS-1: (a) Time-dependent color change when exposing to Cu-K$_\alpha$ X-ray. (b) Electronic absorption spectra before and after irradiation by the Cu-K$_\alpha$ X-ray. (c) EPR spectra before and after irradiation by the Cu-K$_\alpha$ X-ray. (d) Schematic diagram of electron transfer mechanism. (e) Radiochromism imaging.

firmed the generation of radical species after X-ray-induced coloration (Fig. 4c). Therefore, the MV^{2+} guests received electrons upon X-ray irradiation. Similar to reported conclusions, O2 and O7 atoms in carboxyl groups of RCS-1 tend to donate electrons during the coloration process considering the O–N separation (Fig. 4d and Fig. S1c) [46]. The radiochromic behavior gives RCS-1 the ability of radiative imaging. To demonstrate this capability, a sapphire substrate (1.0 × 8.0 × 1.0 mm^3) was prepared as a radiation base using the spin coating method, and a digital template (9.0 × 7.0 mm^2) was selected as the imaging object. As shown in Fig. 4e, when Cu-K$_\alpha$ X-rays from a powder X-ray diffractometer (power: 600 W) were applied to the colorless crystal plate cov-

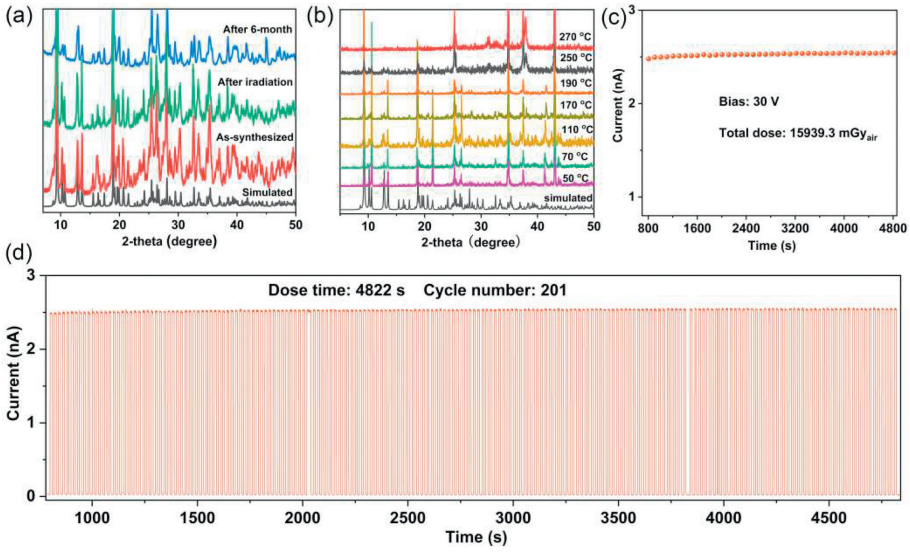

Fig. 5. Physicochemical and X-ray irradiation stability for RCS-1: (a) PXRD patterns before and after standing in air for 6 months. (b) Variable temperature PXRD patterns in the air. (c, d) On/off switching cycles of the photocurrent response.

ered with flat for 30 min, each blue digit appeared on the plate surface.

In practice, radiochromism serves as a crucial method for X-ray detection in addition to direct and indirect electrical detection. The color-changing mode is commonly employed in silver-based radiographic films (requiring the developing and fixing processes) and radiochromic films (without developing and fixing) [11,12]. These films offer portability and high spatial resolution for low-energy X-rays; however, they can only be written on and cannot undergo digital processing. Electrical modes favor digital processing but lack convenience in terms of portability, while the spatial resolution for low-energy X-rays is typically low. Radiochromic semiconductor materials have the unique advantage of simultaneously displaying color changes and electrical signals, thus combining the benefits of both color-changing mode and electrical mode. Radiochromic semiconductors based on photochromic components are ideal candidates for such materials because they can directly exhibit color changes as well as generate electrical signals. The information stored in these semiconductor films can be visually perceived through chromatic aberration or further digitally processed using ordinary electronic card readers (Fig. S6 in Supporting information).

RCS-1 exhibited excellent physicochemical stability. When exposed in air for six months, the PXRD pattern almost remains (Fig. 5a). A TGA analysis reveals that RCS-1 loses 2.9% of its water molecules at 100 °C and has no new loss until 276 °C (Fig. S2 in Supporting information). Despite the loss of water, variable temperature PXRD data from 30 °C to 270 °C demonstrate the stability of crystal structure (Fig. 5b). Except for the physicochemical stability, RCS-1 has also high irradiation stability to X-rays. As shown in Figs. 5c and d, the RCS-1 detector demonstrated consistently stable response even after undergoing 4822 s (~1.34 h) of continuous optoelectrical current switch testing at an extremely dose rate (7.93 mGy_{air}/s) and working bias (30 V). The total dose of 15,939.3 mGy_{air} is equivalent to more than 150,000 times X-ray chests scan with a total dose of 0.1 mGy_{air} per scan.

Apart from exhibiting exceptional detection capabilities in the presence of X-ray radiation, the material also demonstrated stable detection performance even after undergoing discoloration due to Cu-K_α X-ray irradiation. To assess the variation in detection performance before and after exposure to Cu-K_α X-ray radiation from the powder PXRD diffractometer, the irradiated sample pellet detector based on RCS-1 were measured. RCS-1 is radiochromism silent under irradiation of the W X-ray owing to low absorption cross-section. This feature just avoids the occurrence of radiochromism while measuring the as-synthesized sample and benefits to reveal the performance difference between the initial state and the X-ray-induced colored state when exposed under Cu-K_α X-ray.

After X-ray-induced coloration for RCS-1, the σ value remains nearly constant, reaching 8.60×10^{-11} S/cm (Fig. S7 in Supporting information). And the S value still reached 98.73 μC Gy^{-1} cm^{-2} under a bias voltage of 30 V after coloration (Fig. S8 in Supporting information). The $\mu\tau$ of the irradiated sample measured to be 5.49×10^{-4} cm^2/V (Fig. S9 in Supporting information). It is found that there is no attenuation in detection performance for X-ray detection in discoloration detectors even after prolonged exposure to X-ray until color change occurs, indicating that RCS-1 as a radiochromic semiconductive material after coloration still exhibits stable detection performance under X-ray irradiation.

This study presents a radiochromic semiconductor detector for direct X-ray detection, which offers a cost-effective and stability alternative to commercial direct ray detectors. The pellet detector achieved high sensitivity and low dark current, comparable to that of commercial α-Se detectors, while maintaining air, thermal, and long-term X-ray irradiation stability. Additionally, the semiconductor with host-guest strategy utilizing photochromism-active viologen exhibited a rapid color change upon exposure to X-rays, providing an attractive visual detecting ability in addition to electrical signals.

Declaration of competing interest

The authors declare that they have no known competing financial interests or personal relationships that could have appeared to influence the work reported in this paper.

Acknowledgments

We gratefully acknowledge the financial support by the National Key Research and Development Program of Ministry of Science and Technology (No. 2021YFB3801604) and the National Natural Science Foundation (Nos. 22073102, 21827813, 21921001) of China.

Supplementary materials

Supplementary material associated with this article can be found, in the online version, at doi:10.1016/j.cclet.2023.109233.

References

[1] M. Tegze, G. Faigel, Nature 380 (1996) 49–51.
[2] M. Shanmugam, S.V.S. Murty, Y.B. Acharya, et al., Adv. Space Res. 54 (2014) 1974–1984.
[3] J.A. Rowlands, Nature 550 (2017) 47–48.
[4] H. Chen, J. Chen, M. Li, et al., Sci. China Chem. 65 (2022) 2338–2350.
[5] S. Deumel, A. van Breemen, G. Gelinck, et al., Nat. Electron. 4 (2021) 681–688.
[6] B. Sinnott, E. Ron, A.B. Schneider, Endocr. Rev. 31 (2010) 756–773.
[7] W. Wang, J. Lu, X. Xu, et al., Chem. Eng. J. 430 (2022) 133010.
[8] Y. Wang, X. Liu, X. Li, et al., J. Am. Chem. Soc. 141 (2019) 8030–8034.
[9] C. Liang, L. Cheng, S. Zhang, et al., J. Am. Chem. Soc. 144 (2022) 2189–2196.
[10] D.J. Brenner, E.J. Hall, N. Eng, J. Med. 357 (2007) 2277–2284.
[11] M.J. Butson, P.K.N. Yu, T. Cheung, P. Metcalfe, Mater. Sci. Eng. R 41 (2003) 61–120.
[12] S. Devic, Phys. Med. 27 (2011) 122–134.
[13] Y. Han, X. Xu, S. Wang, et al., Chem. Eng. J. 437 (2022) 135468.
[14] L. Ma, S. Guo, Z.M. Zhang, et al., Chin. Chem. Lett. 35 (2024) 108661.
[15] W.J. Cui, S.M. Zhang, Z.Y. Tian, et al., Tungsten 4 (2022) 109–120.
[16] W.Y. Zhang, Y. Lu, Z. Li, et al., Tungsten 4 (2021) 130–137.
[17] L. Wang, Q.Q. He, Q. Gao, et al., Inorg. Chem. 62 (2023) 3799–3807.
[18] Y. Li, B.L. Chai, H. Xu, et al., Inorg. Chem. Front. 9 (2022) 1504–1513.
[19] M.S. Wang, C. Yang, G.E. Wang, et al., Angew. Chem. Int. Ed. 51 (2012) 3432–3435.
[20] M. Xie, J. Lu, B. Li, et al., Chem. Eng. J. 466 (2023) 143272.
[21] L. Cheng, C. Liang, W. Liu, et al., J. Am. Chem. Soc. 142 (2020) 16218–16222.
[22] P. Guo, C. Sun, N. Zhang, et al., Chem. Commun. 54 (2018) 4525–4528.
[23] C. Chen, J. Sun, Y. Zhang, X. Yang, J. Zhang, Angew. Chem. Int. Ed. 56 (2017) 14458–14462.
[24] C. Sun, G. Xu, X. Jiang, et al., J. Am. Chem. Soc. 140 (2018) 2805–2811.
[25] X. Xing, C. Sun, L. Liu, M. Wang, G. Guo, CCS Chem. 3 (2021) 196–203.
[26] C. Sun, X. Yu, M. Wang, G. Guo, Angew. Chem. Int. Ed. 58 (2019) 9475–9478.
[27] X. Yu, C. Sun, B. Liu, M. Wang, G. Guo, Nat. Commun. 11 (2020) 1179.
[28] J. Liu, S. Xia, D. Liu, J. Liu, F. Cheng, CrystEngComm 23 (2021) 850–856.
[29] N.L. Rosi, J. Kim, M. Eddaoudi, et al., J. Am. Chem. Soc. 127 (2005) 1504–1518.
[30] E.R. Johnson, S. Keinan, P. Mori-Sanchez, et al., J. Am. Chem. Soc. 132 (2010) 6498–6506.
[31] C. Ma, H.J. Li, M. Chen, et al., Adv. Funct. Mater. 32 (2022) 2202160.
[32] Y. He, I. Hadar, M.G. Kanatzidis, Nat. Photonics 16 (2022) 14–26.
[33] P. Wang, B. Liu, G. Wang, C. Sun, Inorg. Chem. 61 (2022) 17196–17201.
[34] E.E. Belgin, Radiat. Phys. Chem. 193 (2022) 109960.
[35] L. Sun, S.S. Park, D. Sheberla, M. Dinca, J. Am. Chem. Soc. 138 (2016) 14772–14782.
[36] P. Yu, W. Jie, T. Wang, CrystEngComm 13 (2011) 3521–3525.
[37] M. Zhang, C. Liang, G.D. Cheng, et al., Angew. Chem. Int. Ed. 60 (2021) 9886–9890.
[38] B. Li, M. Xie, J. Lu, et al., Small (2023) 2302492.
[39] C. Liang, S. Zhang, L. Cheng, et al., Angew. Chem. Int. Ed. 59 (2020) 11856–11860.
[40] A. Ruzin, Y. Nemirovsky, J. Appl. Phys. 82 (1997) 4166–4171.
[41] X. Geng, Y. Chen, Y. Li, et al., Adv. Sci. 10 (2023) 2300256.
[42] J. Liu, B. Shabbir, C. Wang, et al., Adv. Mater. 31 (2019) 1901644.
[43] S. Shi, H. Yao, D. Chen, et al., Adv. Opt. Mater. 11 (2023) 2300795.
[44] P.I. Scheurle, A. Maehringer, A.C. Jakowetz, et al., Nanoscale 11 (2019) 20949–20955.
[45] P.S. Braterman, J.I. Song, J. Org. Chem. 56 (1991) 4678–4682.
[46] Y. Han, N. Zhang, M. Wang, G. Guo, J. Phys. Chem. C 124 (2020) 27680–27686.